PAPER

Check for updates

Highly efficient Ni/Ac–Al₂O₃ catalysts in the dry reforming of methane: influence of acetic acid treatment and Ni loading†

Han Xiao, [ID] [ab] Jiaming Dong, [ab] Yimin Zhang, [a] Xiaohua Cao, [ab] Yanhong Li, [ID] [a] Dedong He, [ab] Yongming Luo, [ab] Pingyan Wang*[a] and Hao Wang [ID] *[ab]

The presence of abundant hydroxyl groups on the surface of Al₂O₃ can promote the dispersion of Ni species but produce an inactive NiAl₂O₄ phase at high temperatures. Moreover, the catalysts prepared by the conventional incipient wetness impregnation method lack the sites for the activation of CO₂, which leads to coke deposition and thus affects the catalyst activity. The above restricts the utilization of Ni in conventional Ni/Al₂O₃ catalysts. In this paper, Al₂O₃ support was pre-treated by acetic acid to selectively remove hydroxyl groups without affecting the coordination environment of Al. Results revealed that the Al₂O₃ support after hydroxyl removal not only showed moderate metal–support interaction but also produced more sites for the adsorption and activation of the reactant, which significantly improves the utilization of nickel species and the stability of the catalyst. The conversion of CH₄ and CO₂ at 700 °C was as high as 88% and 90%, respectively, and has an excellent stability of 50 h. This study provides a feasible strategy for the design of highly active methane dry-reforming catalysts.

Introduction

Syngas plays a significant role in the production of varied chemicals.[1–3] Producing syngas by the dry reforming of methane (DRM) with carbon dioxide is a kind of reaction process of natural gas reforming to syngas.[4] The basic principle is that methane (CH₄) reacts with carbon dioxide (CO₂) to produce syngas at high temperatures with the catalyst.[5,6] Syngas generation is a highly thermally absorbent reaction, which usually requires temperatures above 700 °C. The H₂ : CO ratio of syngas produced by the DRM process is approximately 1,[7,8] which is favourable for the synthesis of chemicals.[9–11] Compared to the conventional methane steam reforming process to syngas, the DRM method has remarkable advantages, as follows. (1) The process consumes no water but a large amount of carbon dioxide, reducing energy consumption as well as alleviating greenhouse gas emissions;[12] (2) the feedstock can be attained by a wide range of sources, such as biogas, coke oven gas, coalbed methane, and natural gas;[13,14] (3) two kinds of greenhouse gases are involved in the reaction, which is favourable to the environment; (4)

compared to wet reforming and partial oxidation, it reduces methane consumption by 50%.[15–17] However, during the DRM reaction process (eqn (1)), the high-temperature environment in the reactor inevitably leads to the occurrence of several parallel reactions such as methane decomposition (eqn (2)), inverse Boudouard reaction (eqn (3)), and reverse water-gas shift (RWGS) (eqn (4)).[18–21] These adverse reactions can seriously affect the process efficiency. Coke deposition causes catalyst deactivation and reactor clogging, especially at 550–700 °C, which is a crucial challenge for industrialization. Additionally, the RWGS reaction reduces the H₂/CO molar ratio in syngas,[22,23] affecting the downstream processing of syngas. Therefore, there is an urgent demand to develop a catalyst with superior catalytic activity, resistance to coke deposition and high temperature for DRM.

$$CH_4 + CO_2 \rightarrow 2CO + 2H_2 \; \Delta H^\theta, 298 \text{ K} = 247.3 \text{ kJ mol}^{-1} \quad (1)$$

$$CH_4 \rightarrow C + 2H_2 \; \Delta H^\theta, 298 \text{ K} = 75.0 \text{ kJ mol}^{-1} \quad (2)$$

$$2CO \rightarrow C + CO_2 \; \Delta H^\theta, 298 \text{ K} = -171.0 \text{ kJ mol}^{-1} \quad (3)$$

$$CO_2 + H_2 \rightarrow CO + H_2O \; \Delta H^\theta, 298 \text{ K} = 41.0 \text{ kJ mol}^{-1} \quad (4)$$

Currently, the focus of increased research into the dry reforming of methane catalysts has been mostly on transition metals (*e.g.*, Ni, Fe, and Co)[24,25] and noble metals (*e.g.*, Pd,[26] Pt,[27,28] Rh,[29,30] and Ru[31,32]) catalysts. Among these, noble metals are widely used in DRM based on the high reactivity, stability and excellent resistance to the deposition of coke. With the

[a]*Faculty of Chemical Engineering, Kunming University of Science and Technology, Kunming 650500, P. R. China. E-mail: 972394340@qq.com; haowangfz@foxmail.com*

[b]*The Higher Educational Key Laboratory for Odorous Volatile Organic Compounds Pollutants Control of Yunnan Province, The Innovation Team for Volatile Organic Compounds Pollutants Control and Resource Utilization of Yunnan Province, Kunming University of Science and Technology, Kunming 650500, P. R. China.*

same metal size and active component dispersion, the noble metals Ru and Rh exhibited higher activity compared to active components such as Ni, Pd and Pt.[33] Zhang *et al.* modified nickel-based catalysts by introducing a second metal and using a unique support. This provides new ideas for the widespread use of nickel-based catalysts.[34–37] However, noble metal-based catalysts are not widely industrialized due to the high cost.

Therefore, attention was gradually focused on transition metals with similar catalytic activities as alternative components. Nickel metal (Ni), usually in the form of nanoparticles, has been widely investigated for the catalysis of DRM because of its high hydrocarbon activation capacity and low cost. For example, Tokunaga *et al.* investigated the catalytic activity of Ni, Co, and Fe loaded on Al_2O_3 and found that the catalytic activity of Ni was comparable to that of the noble metal Ru.[38,39] However, Ni-based catalysts are vulnerable to catalyst deactivation owing to the deposition of coke and aggregation of Ni particles at high reaction temperature. Currently, two strategies are proposed to solve this problem. On the one hand, the capacity of CO_2 adsorption and activation is enhanced by adding alkali metals and defect induction.[40,41] On the other hand, the aggregation of Ni particles is inhibited by dispersing Ni on the support with a high specific surface area or tuning the strong interaction between Ni and the support.[42,43] It is reported that Al_2O_3 is widely used as a support for the dry reforming of methane due to its excellent mechanical strength, high thermal stability, tunable surface acidity and alkalinity, and abundant hydroxyl species.[44,45] The abundant hydroxyl groups on the Al_2O_3 surface are favourable for the dispersion of Ni species, but the inactive nickel aluminate phase ($NiAl_2O_4$) is readily generated due to high temperature during the preparation of Ni/Al_2O_3 catalysts and methane dry reforming reaction, which restricts the effective utilization of Ni species and reduces the catalytic activity of methane dry reforming.[46,47] Commercial alumina support without any special treatment lacked vacancy defects for the adsorption and activation of CO_2.[48] Promoting the adsorption and activation of CO_2 molecules in the Ni/Al_2O_3 catalyst for the dry reforming of methane without reducing the utilisation of nickel species is a major challenge in the catalyst design.

Herein, a series of nickel-based alumina catalysts with different Ni loadings and Al_2O_3 support treated with different concentrations of acetic acid were synthesized. The treatment concentration of acetic acid was modulated to remove some of the hydroxyl groups on the Al_2O_3 surface, which can improve the utilization of Ni species and the adsorption and activation of CO_2 molecules. In this paper, the effect of acetic acid treatment on Ni/Al_2O_3 catalysts during the DRM reaction is systematically explored by various characterization results. Meanwhile, insights into the acetic acid treatment strategy might be helpful for the design of new catalysts for the DRM reaction.

Experimental

Catalyst preparation

$Ni(NO_3)_2 \cdot 6H_2O$ (99.0%), commercial $\gamma\text{-}Al_2O_3$, and acetic acid (CH_3COOH, 99.5%) were purchased from Shanghai Aladdin Biochemical Technology Co., Ltd.

Synthesis of acid-treated Al_2O_3

2 g of $\gamma\text{-}Al_2O_3$ was dispersed in a pre-prepared 0.5/1/2 mol L^{-1} solution of 80 mL of CH_3COOH solution, respectively, and stirred continuously for 2 h at 500 rpm. Then, the mixture was centrifuged and washed at pH 7 several times. All of the obtained catalysts were dried in an oven at 100 °C for 4 h and named as xAc–Al_2O_3 (x = 0.5, 1 and 2).

Synthesis of 1Ni/xAc–Al_2O_3 and yNi/Al_2O_3

1Ni/xAc–Al_2O_3 and yNi/Al_2O_3 catalysts were prepared by conventional incipient wetness impregnation method. In a typical procedure, a certain amount of $Ni(NO_3)_2 \cdot 6H_2O$ was dissolved in deionized water under stirring for 2 h. Then, 2 g Al_2O_3 or Ac–Al_2O_3 support was added into the above $Ni(NO_3)_2 \cdot 6H_2O$ solution. The precipitate was dried at 100 °C for 12 h and then calcined in air from room temperature to 700 °C at a ramp rate of 10 °C per minute for 5 h. The obtained samples were denoted as 1Ni/xAc–Al_2O_3 and yNi/Al_2O_3 (x = 0.5, 1, and 2; y = 1, 2, and 5) catalysts, respectively.

Characterization

The detailed methods for X-ray diffraction (XRD), temperature-programmed reduction (H_2-TPR), transmission electron microscopy (TEM), Fourier-transform infrared (FT-IR), X-ray photoelectron spectroscopy (XPS), pyridine-dosing FTIR (Py-FTIR), *in situ* Fourier transform infrared (*in situ* FTIR), *in situ* diffuse reflectance Fourier transform infrared spectroscopy (*in situ* DRIFT), and temperature-programmed desorption of CO_2 (CO_2-TPD) are given in the ESI.†

Catalytic evaluation

The catalytic activity and stability of the xNi/Ac–Al_2O_3 and xNi/Al_2O_3 catalysts in the dry reforming of methane were tested in a fixed-bed flow reactor. 100 mg catalyst (40–60 mesh) was loaded into a quartz reactor and reduced *in situ* at 750 °C by flowing 10 vol% H_2/Ar (30 mL min^{-1}) for 1 h. The reaction gas consisting of CH_4, CO_2 and N_2 ($CH_4 : CO_2 : N_2$ = 1 : 1 : 1) was fed at a GHSV of 36 000 mL h^{-1} g_{cat}^{-1}. The gas products were analysed by an on-line gas chromatograph (GC).

The CH_4/CO_2 conversion and H_2/CO ratio were calculated as follows.

$$CH_4 \ (\%) = \frac{[CH_4]_{in} - [CH_4]_{out}}{[CH_4]_{in}} \times 100 \tag{5}$$

$$CO_2 \ (\%) = \frac{[CO_2]_{in} - [CO_2]_{out}}{[CO_2]_{in}} \times 100 \tag{6}$$

$$H_2/CO = \frac{[H_2]_{out}}{[CO]_{out}} \tag{7}$$

Results and discussion

Catalytic activity measurements

To optimize the concentration for acetic acid treatment and Ni loading, a series of Ni-loaded Al_2O_3 catalysts was prepared by

the impregnation method. Among other things, we carried out warming operations during the continuous feeding process. The resultant activity performance of 1Ni/xAc–Al$_2$O$_3$ (A–C) and yNi/1Ac–Al$_2$O$_3$ (D–F) is shown in Fig. 1. As displayed in Fig. 1A–C, for the 1Ni/xAc–Al$_2$O$_3$ catalysts, three catalysts showed significant differences under treatment with different concentrations of acetic acid. Among them, the 1Ni/1Ac–Al$_2$O$_3$ catalyst exhibited the highest conversion of CH$_4$/CO$_2$, while the 1Ni/0.5Ac–Al$_2$O$_3$ catalyst showed the lowest level of conversion. The H$_2$/CO ratio varies between 0.4 and 0.9 throughout the temperature range and increases with increasing temperature. The trend lines of the 1Ni/1Ac–Al$_2$O$_3$ catalyst and 1Ni/2Ac–Al$_2$O$_3$ catalyst largely overlap, and that of the 1Ni/0.5Ac–Al$_2$O$_3$ catalyst remains lower than that of the other two catalysts. This result identified the optimal acetic acid treatment concentration of 1 mol L^{-1}. Moreover, the catalytic performance of yNi/1Ac–Al$_2$O$_3$ catalysts with different Ni loadings in methane dry reforming reaction was also tested, as shown in Fig. 1D–F. From Fig. 1D–F, it is found that the CH$_4$/CO$_2$ conversion and H$_2$/CO ratios of the three catalysts prepared with different Ni loadings are 5Ni/1Ac–Al$_2$O$_3$ > 2Ni/1Ac–Al$_2$O$_3$ > 1Ni/1Ac–Al$_2$O$_3$ in a descending order. Higher CO$_2$ and CH$_4$ conversions were observed over the 5Ni/1Ac–Al$_2$O$_3$ samples in comparison with those of the xNi/1Ac–Al$_2$O$_3$ samples, indicating that the optimal Ni loading for xNi/1Ac–Al$_2$O$_3$ catalyst is 5 wt%.

The conversions of the yNi/Al$_2$O$_3$ (y = 1, 2, and 5) catalyst and the long-term DRM reaction results of the 5Ni/1Ac–Al$_2$O$_3$ catalyst are shown in Fig. 2 and S1.† It can be seen that the reaction conversions of the 5Ni/Al$_2$O$_3$ catalyst without acetic acid treatment is lower than that of the 5Ni/1Ac–Al$_2$O$_3$ catalyst. However, the catalysts for acetic acid treatment showed obvious advantages in terms of stability, CH$_4$/CO$_2$ conversion rate and H$_2$/CO
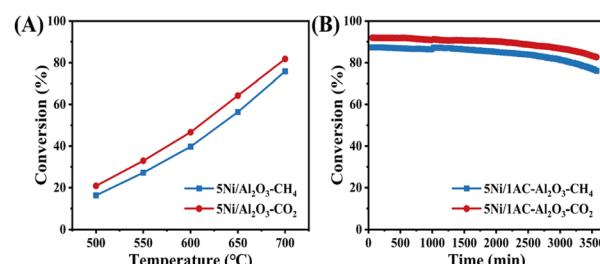

Fig. 2 CH$_4$ and CO$_2$ conversions of 5Ni/Al$_2$O$_3$ (A) and stability test of 5Ni/1Ac–Al$_2$O$_3$ (B). Stability test reaction conditions: $T_{reaction}$ = 700 °C, GHSV = 36 000 mL h^{-1} g$_{cat}$$^{-1}$, CH$_4$/CO$_2$/N$_2$ = 1/1/1.

ratios (Fig. 2B and S1†). In particular, the 5Ni/1Ac–Al$_2$O$_3$ catalyst showed the best performance among all the catalysts. During the 3000 min stability test, it maintained a high conversion rate of 90% and a high H$_2$/CO ratio of 0.97. This indicates that the 5Ni/1Ac–Al$_2$O$_3$ catalyst is extremely stable for the methane dry reforming reaction. It may be a very desirable and reliable choice in production. A comparison of the catalytic performance results revealed that the catalyst treated with acetic acid treatment could maintain the catalytic activity better than the untreated catalyst in the dry reforming of methane. By analysing these data results, it can be concluded that the acetic acid treatment played a positive role in enhancing the catalyst stability and conversion. Further study and exploration of how acetic acid treatment can improve the catalytic performance of the catalyst in the DRM reaction will be very important to further improve the catalyst effect.

We then compared the reaction rate at 700 °C, and the results are shown in Fig. 3. The rates of conversion of CH$_4$ and
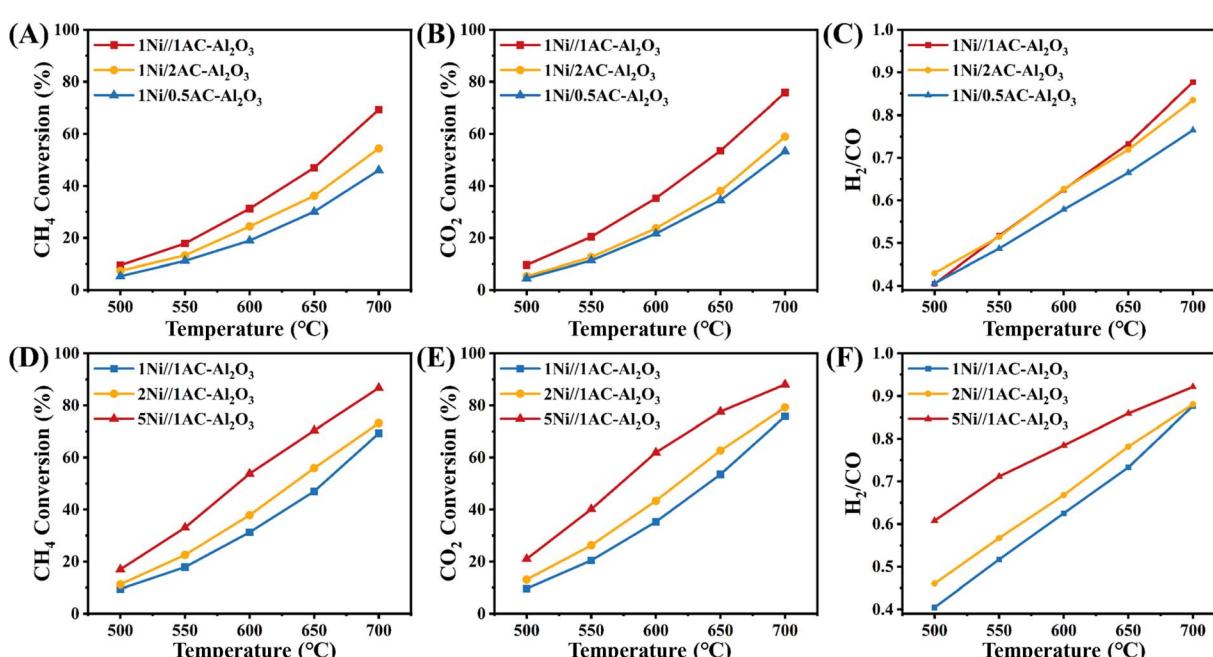
Fig. 1 CH$_4$ and CO$_2$ conversions and H$_2$/CO$_2$ for the dry reforming of methane with 1Ni/xAc–Al$_2$O$_3$ (A–C) and yNi/1Ac–Al$_2$O$_3$ (D–F) (x = 0.5, 1, and 2; y = 1, 2, and 5).
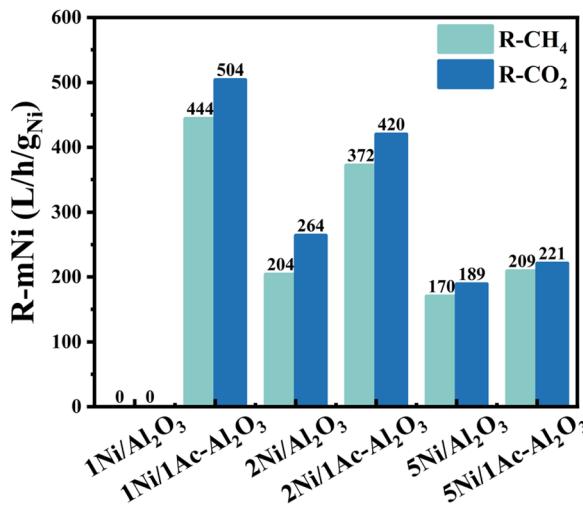
Fig. 3 The CH_4 and CO_2 reaction rate during dry reforming of methane over yNi/1Ac–Al_2O_3 and yNi/Al_2O_3 (y = 1, 2, and 5) at 700 °C.

CO_2 in 1Ni/Al_2O_3 catalyst are almost zero, which can be attributed to the formation on the catalyst surface of the much inactive NiAl$_2$O$_4$ phase (Fig. S2†). However, the acetic acid-treated catalyst of 1Ni/1Ac–Al_2O_3 shows high CH_4 and CO_2 conversion rates and increases from 0 to 444 L_{CH_4} per h per g per Ni and 504 L_{CO_2} per h per g per Ni, respectively. A similar trend is observed in 2Ni/Al_2O_3, 2Ni/1Ac–Al_2O_3 and 5Ni/Al_2O_3, 5Ni/1Ac–Al_2O_3 catalysts.

Apparent activation energy (E_a) experiments were carried out under the conditions of less than 20% conversion. From Fig. 4, the E_a of CH_4 (A) and CO_2 (B) on 5Ni/1Ac–Al_2O_3 and 5Ni/Al_2O_3 catalysts before and after acetic acid treatment was calculated. It can be seen that the E_a of CH_4 and CO_2 on the 5Ni/Al_2O_3 catalyst are 57.39 kJ mol^{-1} and 44.24 kJ mol^{-1}, respectively. However, the E_a values of CH_4 and CO_2 on the acetic acid-treated catalyst of the 5Ni/1Ac–Al_2O_3 catalyst are 44.5 kJ mol^{-1} and 39.6 kJ mol^{-1}, respectively, which are lower than those of the acid-treated 5Ni/Al_2O_3 catalyst. According to the above results, it can be concluded that the acetic acid-treated catalyst is more effective for both CH_4 and CO_2 activation, and the specific reasons for promoting the activation are discussed in a later section.

Effect of acetic acid treatment on the structure of the catalysts

The structure of the unreduced Ac–Al_2O_3 Ac–Al_2O_3, Al_2O_3, yNi/1Ac–Al_2O_3 and yNi/Al_2O_3 (y = 1, 2, and 5) samples was
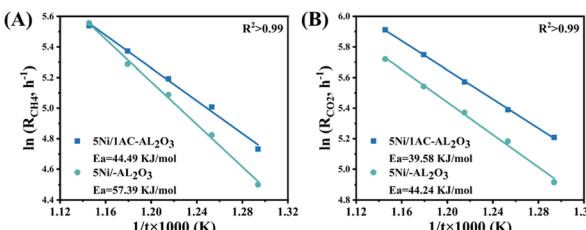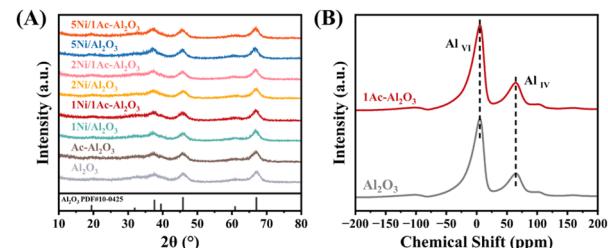
Fig. 5 (A) XRD patterns of the yNi/1Ac–Al_2O_3 and yNi/Al_2O_3 (y = 1, 2, and 5), (B) ^{27}Al NMR spectra over 1Ac–Al_2O_3 and Al_2O_3 samples.

determined by XRD and ^{27}Al-NMR characterization. The XRD patterns are displayed in Fig. 5A. As seen, three distinct reflections at 2θ = 38°, 46°, and 66° were detected, which corresponds to the standard for γ-Al_2O_3 (PDF#10-0425). There were no additional peaks in Fig. 5A after acetic acid treatment, indicating that the structure of these catalysts did not change significantly. Moreover, the diffraction peaks of Ni species were not observed in the XRD results of the yNi/1Ac–Al_2O_3 and yNi/Al_2O_3 (y = 1, 2, and 5) catalysts, suggesting that Ni species were well dispersed on the Al_2O_3 support or formed amorphous phase Ni species.[49,50] Additionally, it can be seen from the TEM images in Fig. S3† that the acetic acid treatment has no significant effect on the morphology of Al_2O_3, which also corresponds to the XRD results before and after the acetic acid treatment in Fig. 5A.

The ^{27}Al NMR data are presented in Fig. 5B; it can be observed that there is no significant change in the peak intensity of ^{27}Al NMR before and after acid treatment. This is because ^{27}Al NMR is a holistic detection technique, and changes in the coordination environment of a few aluminum species cannot be detected. Similar ^{27}Al NMR data can only indicate that acid treatment did not damage the overall structure and morphology of the alumina support, which corresponds to the TEM data.

At the same time, the acidic and functional group changes on the catalyst surface after acetic acid treatment were also investigated. As shown in Fig. 6A, the pyridine adsorption peak at 1450 cm^{-1} is attributed to the Lewis acid sites of xAc–Al_2O_3 (x = 0.5, 1 and 2) and Al_2O_3 samples.[47] With the increase in the acetic acid concentration, the peak gradually decreased, indicating that the Lewis acid sites of the catalyst are reduced. According to reports, Lewis acid sites can be attributed to hydroxyl species or unsaturated coordination metal species,


Fig. 4 CH_4 (A) and CO_2 (B) apparent activation energies over 5Ni/Al_2O_3 and 5Ni/1Ac–Al_2O_3 catalysts.
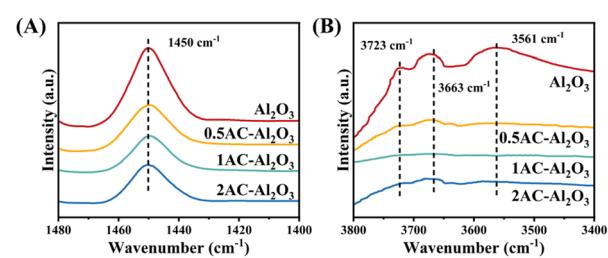
Fig. 6 (A) Py-IR spectra and (B) IR of Al_2O_3, xAc–Al_2O_3 and Al_2O_3 (x = 0.5, 1, and 2).

and nitric acid treatment can remove the hydroxyl group from the surface of Al_2O_3.[47,51]

The process of hydroxyl removal was further confirmed by IR. The IR spectra of hydroxyl groups before and after acetic acid treatment are compared in Fig. 6B. Three peaks at $3723~cm^{-1}$, $3683~cm^{-1}$ and $3561~cm^{-1}$ were observed, corresponding to the surface terminal hydroxyl, bridged hydroxyl, and tri-bridged hydroxyl groups, respectively.[47,52,53] The increase in the acetic acid concentration decreased the intensity of the hydroxyl peaks on the surface of Al_2O_3, indicating that the surface hydroxyl groups were removed by acetic acid treatment. Additionally, a weak bridged hydroxyl peak was observed on the $2Ac/Al_2O_3$ catalyst surface. This may be attributed to the high concentration of acetic acid treatment, resulting in the exposure of the hydroxyl group of the Al_2O_3 bulk phase. Therefore, the hydroxyl group on $2Ac/Al_2O_3$ may interact with Ni to form the nickel aluminate phase, which can justify the weaker activity of $1Ni/2Ac-Al_2O_3$ than that of $1Ni/1Ac-Al_2O_3$. According to the results obtained from pyridine-IR and IR analyses, it has been observed that the reduction of Lewis acid sites after acid treatment can be

attributed to the elimination of hydroxyl groups. Dehydroxylation can reduce the production of nickel aluminate phases, which helps to form more active sites.

Inhibition of $NiAl_2O_4$ phase formation by acetic acid treatment

Fig. 7A compares the H_2-TPR profiles of the $5Ni/1Ac-Al_2O_3$ and $5Ni/Al_2O_3$ catalysts. It can be seen that a significantly reduced peak at 600–800 °C is present, which can be attributed to the reduction of nickel species, and the peak appears at 400–500 °C for $5Ni/1Ac-Al_2O_3$ due to the reduction of NiO with intermediate size.[54] The reduction peak shifted to lower temperature after acetic acid treatment, indicating that the interaction between metal Ni and the Al_2O_3 support was weakened, and the Ni species were more easily reduced. Therefore, the $5Ni/1Ac-Al_2O_3$ catalyst has more active phases, resulting in higher catalytic activity, which is consistent with the activity data.

Similar results were confirmed by the XPS characterization. The Ni 2p XPS spectra of $5Ni/1Ac-Al_2O_3$ and $5Ni/Al_2O_3$ are illustrated in Fig. 7B. According to literature, the peaks at 852.5 eV, 855.9 eV, and 857.5 eV are attributed to Ni^0, Ni_{oct}^{2+} (Ni^{2+} in octahedral coordination sites), and Ni_{tet}^{2+} (Ni^{2+} in tetrahedral coordination sites), respectively.[55–58] Ni_{oct}^{2+} and Ni_{tet}^{2+} are Ni species with strong metal–support interaction and difficult to reduce. For the $5Ni/Al_2O_3$ sample, the contents of Ni^0, Ni_{oct}^{2+}, and Ni_{tet}^{2+} are 2.04%, 43.09%, and 16.11%, respectively. For the $Ni/1Ac-Al_2O_3$ sample, the contents of Ni^0, Ni_{oct}^{2+}, and Ni_{tet}^{2+} are 4.11%, 42.59%, and 14.79%, respectively. Although small Ni^0 species may be oxidized due to off-line reduction, it is still observed that after acetic acid treatment, the content of Ni species in the strong metal–support interaction decreases and the content of Ni^0 increases. The possible
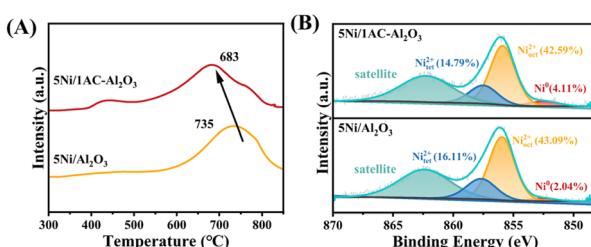

Fig. 7 H_2-TPR profiles (A) and XPS spectra (B) over the $5Ni/1Ac-Al_2O_3$ and $5Ni/Al_2O_3$ catalysts.
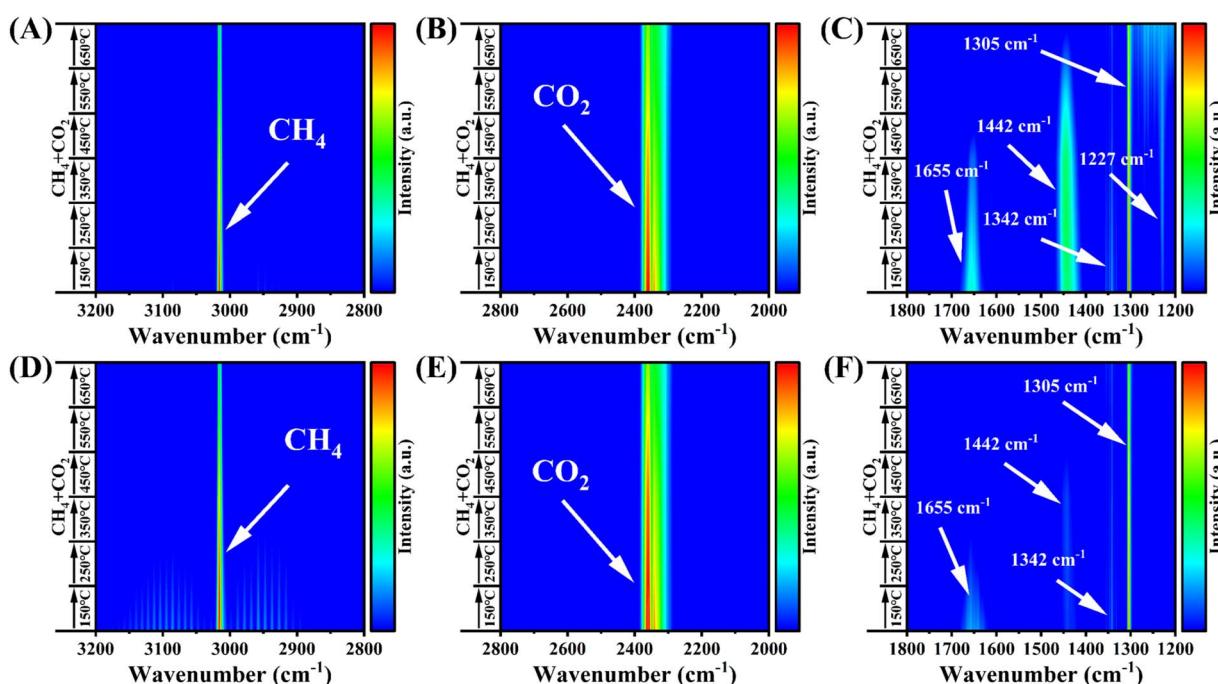
Fig. 8 *In situ* DRIFTS spectra of $5Ni/1Ac-Al_2O_3$ (A–C) and $5Ni/Al_2O_3$ (D–F) catalysts.

reason is that acetic acid treatment decreases the number of hydroxyl groups on the Al_2O_3 support, which is conducive to the reduction of Ni species and improves the activity of the catalyst in DRM.

Acetic acid treatment promotes the adsorption and activation of CO_2

In situ DRIFTS experiments of reactants were carried out to further identify the intermediate species and compare with the activation abilities of CO_2 and CH_4 on the $5Ni/Ac–Al_2O_3$ (Fig. 8A–C) and $5Ni/Al_2O_3$ (Fig. 8D–F) catalysts. Both catalysts show peaks located at 3016 cm^{-1} and 1305 cm^{-1}, which are attributed to the gas phase CH_4, as well as another broad one at $\sim$2360 cm^{-1} corresponding to the deformation vibration of gas phase CO_2 is observed.[59–61] Notably, the signals attributed to CH_4 and CO_2 in the $5Ni/1Ac–Al_2O_3$ catalyst weaken at lower temperatures compared to the $5Ni/Al_2O_3$ catalyst, indicating that the activation capacity for the reactants of the $5Ni/1Ac–Al_2O_3$ catalysts is greater. This is probably because the $5Ni/1Ac–Al_2O_3$ samples have more active sites. The signals corresponding to the reaction intermediates appear from 1200 cm^{-1} to 1800 cm^{-1} (Fig. 8C and F). Two signals located at 1442 cm^{-1} and 1342 cm^{-1} can be attributed to the deformation vibrations of the CH_3^* species,[62,63] and two other bands at 1655 cm^{-1} and 1227 cm^{-1} appear, which are attributed to bicarbonate and carbonate, respectively.[64,65] The CH_3^* species are produced by the activation of methane, while the oxygen-containing species (bicarbonate) can be produced by the activation of CO_2.[59,66] Additionally, it can be observed that the intermediate signals on the $5Ni/1Ac–Al_2O_3$ catalyst is stronger than that on the $5Ni/Al_2O_3$ catalyst. This is because the $5Ni/1Ac–Al_2O_3$ catalyst has more active sites after being treated with acetic acid; thus, its ability to activate the reactants is better than that of the $5Ni/Al_2O_3$ catalyst.

To further prove the CO_2 activation capacity over the $5Ni/1Ac–Al_2O_3$ catalyst, CO_2-TPD characterization was carried out,

Fig. 9 CO_2-TPD patterns over Al_2O_3, $1Ac–Al_2O_3$, $5Ni/Al_2O_3$ and $5Ni/1Ac–Al_2O_3$.

as shown in Fig. 9. It can be seen that all the samples show a low temperature adsorption peak at about 100 °C, which could be attributed to the adsorption of CO_2 by the supports,[67] and the CO_2 adsorption signal at 200–500 °C can be attributed to the impregnated Ni species.[68] The acetic acid-treated $1Ac/Al_2O_3$, $5Ni/1Ac–Al_2O_3$ exhibits strong CO_2 absorption peaks in the 200–500 °C range, whereas no obvious CO_2 absorption peaks are observed over the non-acid-treated Al_2O_3, $5Ni/Al_2O_3$ in the same range. This confirms that the acetic acid-treated catalyst facilitates the adsorption and activation of CO_2, corresponding to the *in situ* DRIFTS results.

Conclusions

In summary, a strategy to directly remove hydroxyl groups from the surface of alumina support has been developed. The hydroxyl species can be removed by simple acetic acid treatment, inhibiting the formation of $NiAl_2O_4$ and significantly improving the utilization efficiency of the nickel species, thereby enhancing the catalytic activity. Additionally, the catalyst after acetic acid treatment promoted the activation of CO_2. This study provides a feasible approach for nickel-based alumina catalysts to undergo the methane dry-reforming methane reaction through simple acetic acid treatment.

Data availability

Data will be made available on request to the corresponding author.

Author contributions

Han Xiao: methodology, writing – original draft. Jiaming Dong: writing – original draft. Yimin Zhang: conceptualization. Xiaohua Cao: writing-review & editing. Yanhong Li: formal analysis. Dedong He: conceptualization, investigation. Yongming Luo: methodology, investigation. Pingyan Wang: supervision, investigation. Hao Wang: supervision, writing-review & editing.

Conflicts of interest

There are no conflicts to declare.

Acknowledgements

Notes and references

1 A. Kurlov, E. B. Deeva, P. M. Abdala, D. Lebedev, A. Tsoukalou, A. Comas-Vives, A. Fedorov and C. R. Müller, *Nat. Commun.*, 2020, **11**, 4920.

2 H. K. Min, S. Kweon, Y. W. Kim, H. An, D. Jo, E. D. Park, C. H. Shin and M. B. Park, *Appl. Catal., B*, 2021, **298**, 120627.

3 Y. Song, E. Ozdemir, S. Ramesh, A. Adishev, S. Subramanian, A. Harale, M. Albuali, B. A. Fadhel, A. Jamal, D. Moon, S. H. Choi and C. T. Yavuz, *Science*, 2020, **367**, 777–781.

4 H. Qu, H. Yang, L. B. Han, S. H. He, J. D. Liu, R. J. Hu, H. Q. Su and Y. Su, *Chem. Eng. J.*, 2023, **453**, 139694.

5 K. H. Han, S. Wang, N. Hu, W. D. Shi and F. G. Wang, *ACS Appl. Mater. Interfaces*, 2022, **14**, 23487–23495.

6 L. Wang and F. G. Wang, *Energy Fuels*, 2022, **36**, 5594–5621.

7 Y. Tang, Y. C. Wei, Z. Y. Wang, S. R. Zhang, Y. T. Li, L. Nguyen, Y. X. Li, Y. Zhou, W. J. Shen, F. F. Tao and P. J. Hu, *J. Am. Chem. Soc.*, 2019, **141**, 7283–7293.

8 A. S. Al-Fatesh, R. Kumar, S. O. Kasim, A. A. Ibrahim, A. H. Fakeeha, A. E. Abasaeed, R. Alrasheedu, A. Bagabas, M. L. Chaudhary, F. Frusteri and B. Chowdhury, *Catal. Today*, 2020, **348**, 236–242.

9 S. Dama, S. R. Ghodke, R. Bobade, H. R. Gurav and S. Chilukuri, *Appl. Catal., B*, 2018, **224**, 146–158.

10 A. T. Ashcroft, A. K. Cheetham, M. L. H. Green and P. D. F. Vernon, *Nature*, 1991, **352**, 225–226.

11 S. T. Oyama, P. Hacarlioglu, Y. F. Gu and D. Lee, *Int. J. Hydrogen Energy*, 2012, **37**, 10444–10450.

12 X. Y. Gao, J. Ashok, S. Widjaja, K. Hidajat and S. Kawi, *Appl. Catal., A*, 2015, **503**, 34–42.

13 W. H. Chen, C. L. Hsu and S. W. Du, *Energy*, 2015, **86**, 758–771.

14 Q. Yi, G. S. Wu, M. H. Gong, Y. Huang, J. Feng, Y. H. Hao and W. Y. Li, *Appl. Energy*, 2017, **193**, 149–161.

15 X. Y. Gao, Z. T. Lin, T. T. Li, L. T. Huang, J. M. Zhang, S. Askari, N. Dewangan, A. Jangam and S. Kawi, *Catalysts*, 2021, **11**, 455.

16 L. C. Buelens, V. V. Galvita, H. Poelman, C. Detavernier and G. B. Marin, *Science*, 2016, **354**, 449–452.

17 I. V. Yentekakis, P. Panagiotopoulou and G. Artemakis, *Appl. Catal., B*, 2021, **296**, 120210.

18 K. K. Bu, J. Deng, X. Y. Zhang, S. Kuboon, T. T. Yan, H. R. Li, L. Y. Shi and D. S. Zhang, *Appl. Catal., B*, 2020, **267**, 118692.

19 J. Martin-del-Campo, M. Uceda, S. Coulombe and J. Kopyscinski, *J. CO2 Util.*, 2021, **46**, 101474.

20 B. Yang, J. Deng, H. R. Li, T. T. Yan, J. P. Zhang and D. S. Zhang, *Iscience*, 2021, **24**, 102747.

21 Y. Wang, L. Yao, S. H. Wang, D. H. Mao and C. W. Hu, *Fuel Process. Technol.*, 2018, **169**, 199–206.

22 G. J. Zhang, J. W. Liu, Y. Xu and Y. H. Sun, *Int. J. Hydrogen Energy*, 2018, **43**, 15030–15054.

23 M. M. Barroso-Quiroga and A. E. Castro-Luna, *Int. J. Hydrogen Energy*, 2010, **35**, 6052–6056.

24 A. M. O'Connor, Y. Schuurman, J. R. H. Ross and C. Mirodatos, *Catal. Today*, 2006, **115**, 191–198.

25 S. Therdthianwong, A. Therdthianwong, C. SiangChin and S. Yonprapat, *Int. J. Hydrogen Energy*, 2008, **33**, 991–999.

26 S. Damyanova, B. Pawelec, K. Arishtirova, J. L. G. Fierro, C. Sener and T. Dogu, *Appl. Catal., B*, 2009, **92**, 250–261.

27 P. G. Schulz, M. G. Gonzalez, C. E. Quincoces and C. E. Gigola, *Ind. Eng. Chem. Res.*, 2005, **44**, 9020–9029.

28 H. Y. Wang and E. Ruckenstein, *Appl. Catal., A*, 2000, **204**, 143–152.

29 R. Wang, H. Y. Xu, X. B. Liu, Q. J. Ge and W. Z. Li, *Appl. Catal., A*, 2006, **305**, 204–210.

30 C. Carrara, J. Múnera, E. A. Lombardo and L. M. Cornaglia, *Top. Catal.*, 2008, **51**, 98–106.

31 J. X. Chen, C. C. Yao, Y. Q. Zhao and P. H. Jia, *Int. J. Hydrogen Energy*, 2010, **35**, 1630–1642.

32 D. L. Li, R. L. Li, M. M. Lu, X. Y. Lin, Y. Y. Zhan and L. L. Jiang, *Appl. Catal., B*, 2017, **200**, 566–577.

33 D. Pakhare, C. Shaw, D. Haynes, D. Shekhawat and J. Spivey, *J. CO2 Util.*, 2013, **1**, 37–42.

34 J. J. Zheng, S. Impeng, J. Liu, J. Deng and D. S. Zhang, *Appl. Catal., B*, 2024, **342**, 123369.

35 X. Y. Zhang, J. Deng, T. W. Lan, Y. J. Shen, Q. D. Zhong, W. Ren and D. S. Zhang, *ACS Catal.*, 2022, **12**, 14152–14161.

36 X. Y. Zhang, J. Deng, M. Pupucevski, S. Impeng, B. Yang, G. R. Chen, S. Kuboon, Q. D. Zhong, K. Faungnawakij, L. R. Zheng, G. Wu and D. S. Zhang, *ACS Catal.*, 2021, **11**, 12087–12095.

37 J. Deng, M. Gao, J.-y. Hasegawa, X. Zhang, A. Wang, A. Chen and D. Zhang, *CCS Chem.*, 2023, **5**, 2111–2124.

38 O. Tokunaga, Y. Osada and S. Ogasawara, *Fuel*, 1989, **68**, 990–994.

39 O. Tokunaga and S. Ogasawara, *React. Kinet. Catal. Lett.*, 1989, **39**, 69–74.

40 C. Crisafulli, S. Scirè, S. Minicò and L. Solarino, *Appl. Catal., A*, 2002, **225**, 1–9.

41 N. Oyama, Y. Iwami, T. Yamamoto, S. Machida, T. Higuchi, H. Sato, M. Sato, K. Takeda, Y. Watanabe, M. Shimizu and K. Nishioka, *ISIJ Int.*, 2011, **51**, 913–921.

42 T. Huang, W. Huang, J. Huang and P. Ji, *Fuel Process. Technol.*, 2011, **92**, 1868–1875.

43 E. García-Bordejé, A. B. Dongil, J. M. Conesa, A. Guerrero-Ruiz and I. Rodríguez-Ramos, *Chem. Eng. J.*, 2023, **472**, 144953.

44 Z. A. Xie, Z. Li, P. Tang, Y. Y. Song, Z. Zhao, L. A. Kong, X. Q. Fan and X. Xiao, *J. Catal.*, 2021, **397**, 172–182.

45 T. Margossian, K. Larmier, S. M. Kim, F. Krumeich, A. Fedorov, P. Chen, C. R. Müller and C. Copéret, *J. Am. Chem. Soc.*, 2017, **139**, 6919–6927.

46 S. S. Zhang, M. Ying, J. Yu, W. C. Zhan, L. Wang, Y. Guo and Y. L. Guo, *Appl. Catal., B*, 2021, **291**, 120074.

47 Y. M. Zhang, Y. Zu, D. D. He, J. Liang, L. H. Zhu, Y. Mei and Y. M. Luo, *Appl. Catal., B*, 2022, **315**, 121539.

48 K. Li, C. L. Pei, X. Y. Li, S. Chen, X. H. Zhang, R. Liu and J. L. Gong, *Appl. Catal., B*, 2020, **264**, 118448.

49 Z. J. Huang, D. D. He, W. H. Deng, G. W. Jin, K. Li and Y. M. Luo, *Nat. Commun.*, 2023, **14**, 100.

50 L. Zhang, S. J. Wu, Y. Zhang, T. H. Ai, D. K. Chen, Y. M. Luo and D. D. He, *Chem. Eng. J.*, 2024, **486**, 150337.

51 K. Hadjiivanov, in *Advances in Catalysis*, ed. F. C. Jentoft, Academic Press, 2014, vol. 57, pp. 99–318.

52 T. Cao, R. You, X. Y. Zhang, S. L. Chen, D. Li, Z. H. Zhang and W. X. Huang, *Phys. Chem. Chem. Phys.*, 2018, **20**, 9659–9670.

53 J. J. Dai and H. B. Zhang, *J. Catal.*, 2022, **410**, 266–279.

54 Y. Bai, D. Y. Shen, G. W. Yu, J. Wang, S. A. Lyu, Y. H. Zhang, G. H. Wang, J. L. Li and L. Li, *New J. Chem.*, 2023, **47**, 17186–17193.

55 S. Q. Li, Y. Fu, W. B. Kong, B. R. Pan, C. K. Yuan, F. F. Cai, H. Zhu, J. Zhang and Y. H. Sun, *Appl. Catal., B*, 2020, **277**, 118921.

56 P. Yan, S. Xi, H. Peng, D. R. G. Mitchell, L. Harvey, M. Drewery, E. M. Kennedy, Z. Zhu, G. Sankar and M. Stockenhuber, *J. Am. Chem. Soc.*, 2023, **145**, 9718–9728.

57 P. H. Yan, X. X. Tian, E. M. Kennedy and M. Stockenhuber, *Catal. Sci. Technol.*, 2022, **12**, 2184–2196.

58 Y. Zhang, R. Zeng, Y. Zu, L. Zhu, Y. Mei, Y. Luo and D. He, *Chin. J. Chem. Eng.*, 2022, **48**, 76–90.

59 H. Wang, G. Q. Cui, H. Lu, Z. Y. Li, L. Wang, H. Meng, J. Li, H. Yan, Y. S. Yang and M. Wei, *Nat. Commun.*, 2024, **15**, 3765.

60 P. Yan, H. Peng, X. Zhang, H. Rabiee, M. Ahmed, Y. Weng, A. Rozhkovskaya, J. Vogrin, M. Konarova and Z. Zhu, *Fuel*, 2024, **374**, 132373.

61 D. He, J. Yan, K. Chen, L. Zhang, J. Lu, J. Liu and Y. Luo, *ACS Catal.*, 2023, **13**, 12114–12124.

62 Y. Wang, L. Li, G. Y. Li, Q. Zhao, X. S. Wu, Y. N. Wang, Y. F. Sun and C. W. Hu, *ACS Catal.*, 2023, **13**, 6486–6496.

63 G. X. Deng, G. F. Zhang, X. Zhu, Q. J. Guo, X. B. Liao, X. Chen and K. Z. Li, *Appl. Catal., B*, 2021, **289**, 120033.

64 Q. S. Pan, J. X. Peng, S. Wang and S. D. Wang, *Catal. Sci. Technol.*, 2014, **4**, 502–509.

65 L. Azancot, L. F. Bobadilla, M. A. Centeno and J. A. Odriozola, *Appl. Catal., B*, 2021, **285**, 119822.

66 D. D. He, S. J. Wu, X. H. Cao, D. K. Chen, L. Zhang, Y. Zhang and Y. M. Luo, *Applied Catalysis B: Environment and Energy*, 2024, **346**, 123728.

67 P. Yan, H. Peng, X. Wu, H. Rabiee, Y. Weng, M. Konarova, J. Vogrin, A. Rozhkovskaya and Z. Zhu, *J. Catal.*, 2024, **432**, 115439.

68 C. Sun, P. Beaunier and P. Da Costa, *Catal. Sci. Technol.*, 2020, **10**, 6330–6341.